PET Imaging of Cholinergic Neurotransmission in Neurodegenerative Disorders

Solveig Tiepolt*[1], Philipp M. Meyer*[1], Marianne Patt[1], Winnie Deuther-Conrad[2], Swen Hesse[1], Henryk Barthel[1], and Osama Sabri[1]

[1]*Department of Nuclear Medicine, University of Leipzig, Leipzig, Germany; and* [2]*Helmholtz-Zentrum Dresden-Rossendorf, Research Site Leipzig, Leipzig, Germany*

As a neuromodulator, the neurotransmitter acetylcholine plays an important role in cognitive, mood, locomotor, sleep/wake, and olfactory functions. In the pathophysiology of most neurodegenerative diseases, such as Alzheimer disease (AD) or Lewy body disorder (LBD), cholinergic receptors, transporters, or enzymes are involved and relevant as imaging targets. The aim of this review is to summarize current knowledge on PET imaging of cholinergic neurotransmission in neurodegenerative diseases. For PET imaging of presynaptic vesicular acetylcholine transporters (VAChT), (−)-^{18}F-fluoroethoxybenzovesamicol (^{18}F-FEOBV) was the first PET ligand that could be successfully translated to clinical application. Since then, the number of ^{18}F-FEOBV PET investigations on patients with AD or LBD has grown rapidly and provided novel, important findings concerning the pathophysiology of AD and LBD. Regarding the α4β2 nicotinic acetylcholine receptors (nAChRs), various second-generation PET ligands, such as ^{18}F-nifene, ^{18}F-AZAN, ^{18}F-XTRA, (−)-^{18}F-flubatine, and (+)-^{18}F-flubatine, were developed and successfully translated to human application. In neurodegenerative diseases such as AD and LBD, PET imaging of α4β2 nAChRs is of special value for monitoring disease progression and drugs directed to α4β2 nAChRs. For PET of α7 nAChR, ^{18}F-ASEM and ^{11}C-MeQAA were successfully applied in mild cognitive impairment and AD, respectively. The highest potential for α7 nAChR PET is seen in staging, in evaluating disease progression, and in therapy monitoring. PET of selective muscarinic acetylcholine receptors (mAChRs) is still in an early stage, as the development of subtype-selective radioligands is complicated. Promising radioligands to image mAChR subtypes M1 (^{11}C-LSN3172176), M2 (^{18}F-FP-TZTP), and M4 (^{11}C-MK-6884) were developed and successfully translated to humans. PET imaging of mAChRs is relevant for the assessment and monitoring of therapies in AD and LBD. PET of acetylcholine esterase activity has been investigated since the 1990s. Many PET studies with ^{11}C-PMP and ^{11}C-MP4A demonstrated cortical cholinergic dysfunction in dementia associated with AD and LBD. Recent studies indicated a solid relationship between subcortical and cortical cholinergic dysfunction and noncognitive dysfunctions such as balance and gait in LBD. Taken together, PET of distinct components of cholinergic neurotransmission is of great interest for diagnosis, disease monitoring, and therapy monitoring and to gain insight into the pathophysiology of different neurodegenerative disorders.

Key Words: neurology; PET; acetylcholine; Alzheimer disease; Lewy body disorder; neurodegenerative disorder; PET

J Nucl Med 2022; 63:33S–44S
DOI: 10.2967/jnumed.121.263198

Essential processes such as neuroplasticity, neuronal synchronization, and connectivity are modulated by the neurotransmitter acetylcholine, which is accordingly critically involved in and highly relevant to cognitive, mood, locomotor, sleep/wake, and olfactory functions (*1,2*). The cholinergic system in the central nervous system (CNS) consists of 2 major projections: the first is from the basal forebrain (Ch1 to Ch4 cholinergic groups) to the cortex, amygdala, hippocampus, and olfactory bulb, and the second is from the brain stem (Ch5 and Ch6 cholinergic groups) to the thalamus and other brain stem nuclei. There are also intrinsic striatal, cortical, and cerebellar cholinergic neurons (*1,3,4*).

In the synapse of the presynaptic cholinergic neuron, acetylcholine is synthetized by the choline acetyltransferase from choline and acetyl coenzyme A. Acetylcholine is transported via the vesicular acetylcholine transporter (VAChT) into the presynaptic vesicles of the cholinergic nerve terminals, where it is stored for future release. Released acetylcholine binds to and activates nicotinic and muscarinic acetylcholine receptors (nAChRs and mAChRs). Acetylcholine esterase (AChE) rapidly clears the synaptic cleft of acetylcholine by enzymatic hydrolysis to acetate and choline. Choline undergoes a recycling reuptake by the presynaptic high-affinity choline transporter (Fig. 1) (*2–4*).

In 1982, Bartus et al. published the cholinergic hypothesis of Alzheimer disease (AD), which described the loss of memory as a result of cortical and basal forebrain cholinergic dysfunction (*5*). This hypothesis was convincingly confirmed because anticholinergic drugs could be proved to induce cognitive impairment (*3,6*) whereas AChE inhibitors could be proved to induce the opposite (*3*).

The cholinergic pathophysiology of the 2 most prevalent neurodegenerative disorders—AD and LBD spectrum (the latter including Parkinson disease [PD], PD with dementia [PDD], and Lewy body dementia [DLB])—differs between each other. AD shows cholinergic dysfunction and loss of neurons in the basal forebrain, likely in close relationship to the relevant loss of cholinergic cortical axons from tau and amyloid proteinopathy. However, cholinergic striatal interneurons and cholinergic innervation of the thalamus receiving innervation from the brain stem are preserved (*4*). In contrast, LBD, likely in close association with α-synucleinopathy, shows cholinergic dysfunction and degeneration not only in the basal forebrain but also in the brain stem. In LBD, this more complex subcortical and cortical neuropathology and cholinergic

Received Mar. 23, 2022; revision accepted May 6, 2022.
For correspondence or reprints, contact Osama Sabri (osama.sabri@medizin.uni-leipzig.de).
*Contributed equally to this work.

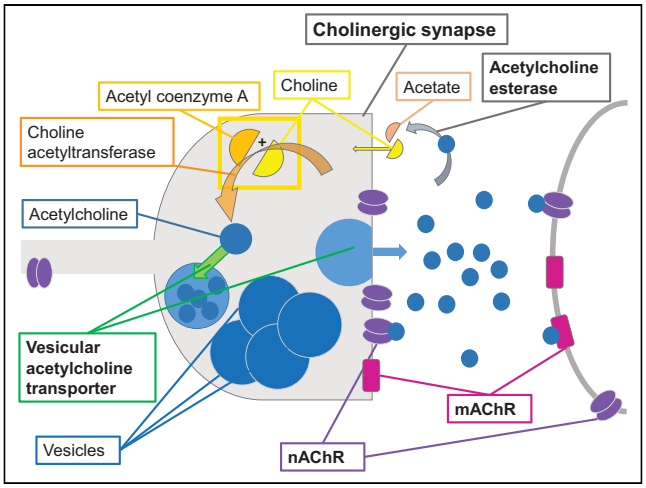

FIGURE 1. Cholinergic synapse: physiologic processes. In synapse of presynaptic cholinergic neuron, acetylcholine is synthetized by choline acetyltransferase from choline and acetyl coenzyme A. It is then stored in vesicles in very high concentrations. This storage process, as well as release of acetylcholine in synaptic cleft, is mediated by VAChT. Released acetylcholine binds to and activates nAChRs and mAChRs and, in case of postsynaptic receptors, transports signal to next neuron. AChE rapidly clears synaptic cleft of acetylcholine. This enzyme hydrolyzes acetylcholine to acetate and choline. The latter undergoes recycling reuptake into the presynaptic nerve terminal.

dysfunction are associated with and most likely explain the wide spectrum of motor and various nonmotor symptoms in LBD (*3,4*). Novel neuropathologic and cholinergic PET findings in the brain and body of LBD patients, especially the gut—present also in early or prodromal PD—led to a paradigm shift in our understanding of the pathophysiology of LBD and to the definition of body-first and brain-first LBD subtypes (*7,8*).

The possibility of obtaining in vivo information about the integrity of cholinergic transmission by means of PET imaging is of major interest in studying the pathophysiology of various neurodegenerative disorders such as AD and LBD and has major relevance in cholinergic drug development. This option refers to all the different compartments of this complex neurotransmitter system. The aim of this review is to summarize the current knowledge on PET imaging of cholinergic transmission, including imaging of VAChT, nAChRs, mAChRs, and AChE in neurodegenerative diseases.

VAChT

Structure and Distribution of VAChT

VAChT is an approximately 500-amino-acid polypeptide uniquely present in cholinergic nerve terminals of the central and peripheral nervous system and corresponding closely to choline acetyltransferase (*9*).

Radioligands for Imaging VAChT

Many VAChT PET ligands have been generated (*9*). Vesamicol was used as the lead compound. The development of vesamicol derivatives showing high affinity to VAChT and high selectivity over off-targets such as σ-receptors was challenging. Several vesamicol-, trozamicol-, and benzovesamicol-based PET ligands, as well as morpholinovesamicols and other vesamicol analogs, were developed and tested preclinically (*9*). Only the PET ligand (−)-^{18}F-fluoroethoxybenzovesamicol (^{18}F-FEOBV) (Table 1; Fig. 2A) and the SPECT tracer (−)-5-^{123}I-iodobenzovesamicol (^{123}I-IBVM)

TABLE 1
Most Relevant VAChT PET (SPECT) Radioligands

Tracer name	Formula
^{123}I-IBVM	(−)-5-^{123}I-iodobenzovesamicol
(−)-^{18}F-FEOBV	(2*R*,3*R*)-5-^{18}F-fluoroethoxy-benzovesamicol
^{18}F-VAT	(−)-(1-(8-(2-^{18}F-fluoroethoxy)-3-hydroxy-1,2,3,4-tetrahydronaphthalen-2-yl)-piperidin-4-yl)(4-fluorophenyl) methanone

(Table 1; Fig. 2A) were successfully transferred to clinical application (*10,11*). According to validation in preclinical studies and human postmortem brain (*12–14*), ^{18}F-FEOBV showed favorable characteristics for in vivo assessment of VAChT in healthy controls (HCs) (*15*). The pattern of distribution of the radioligand corresponded to the known heterogeneous organization of cholinergic projections in the human brain with the following rank order: striatum > thalamus > cerebellar vermis > amygdala–hippocampus complex > brain stem > cerebral cortex (*15,16*). Aging was associated with a decline in VAChT binding by 4% per decade within the striatum and approximately 3% per decade within the thalamus, anterior cingulate cortex, and premotor cortex (*16*). In addition to full kinetic modeling to calculate the distribution volume or binding potential of ^{18}F-FEOBV, simplified approaches to VAChT quantification were validated using delayed static PET scans and reference regions such as the cerebellar cortex or white matter (*15,17,18*).

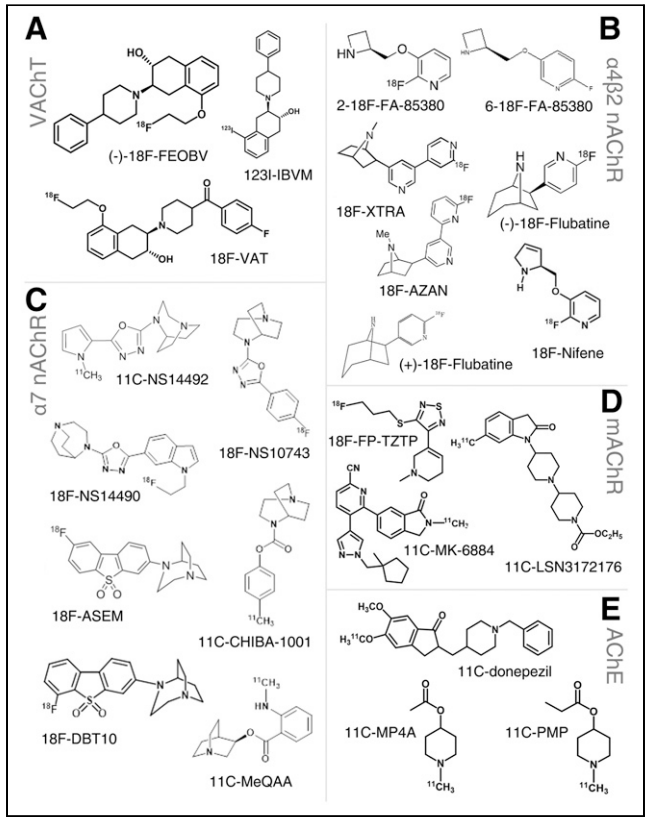

FIGURE 2. Names and structural chemical formulas of most relevant radioligands for distinct cholinergic targets.

^{18}F-VAT is a benzovesamicol-based VAChT PET ligand (Table 1; Fig. 2A). Recent in vitro, preclinical in vivo, and postmortem human brain findings were promising (*19,20*). A ^{18}F-VAT PET trial in humans is under way.

VAChT PET Imaging Results in Neurodegeneration

The first in vivo VAChT imaging study of the brain in AD, PD, PDD, and HC was performed by Kuhl et al. using ^{123}I-IBVM SPECT. Compared with HCs, a widespread decrease in VAChT binding within the neocortex and hippocampus has been detected in PDD and early-onset AD (EOAD) (*21*). In contrast, in late-onset AD (LOAD), the VAChT decline was restricted to the temporal cortex and was less pronounced, indicating a distinct vulnerability of the basal forebrain in EOAD and LOAD (*21,22*). Of interest, in mild to moderate AD, as assessed by the clinical dementia rating scale, cortical VAChT binding was more declined in EOAD than in LOAD. In severe AD, VAChT binding was decreased to a similar degree in EOAD and LOAD. In Lewy body dementia (DLB), compared with HCs, ^{123}I-IBVM SPECT showed a decrease in VAChT in Ch4 and pedunculopontine thalamic (Ch5) projections and within striatal interneurons. In contrast, septohippocampal cholinergic projections were spared (*23*). Thus, the pattern of cortical and subcortical cholinergic dysfunction in DLB differs from that in AD.

By ^{18}F-FEOBV PET, lower VAChT binding in cholinergic terminals within the frontotemporoparietal and cingulate cortices has been detected in AD in comparison with HCs, as is presumed to reflect a characteristic caudorostral dysfunction of the nucleus basalis of Meynert (Ch4; Figs. 3A–3D) (*17,22*). Reduced cortical VAChT in AD was significantly associated with global cognitive dysfunction. In the same AD patients, ^{18}F-FEOBV PET was more sensitive in detecting AD-related changes than was ^{18}F-FDG PET or β-amyloid PET (*17*). In DLB, there was a widespread decrease in VAChT binding in the frontotemporoparietal and occipital cortices, hippocampus, amygdala, and thalamus (−17% to −21%; Fig. 3E) (*18*). In PD, the relationship between disturbances in VAChT binding and motor symptoms such as falls and freezing of gait as part of the postural instability gait disturbance subtype were investigated (*22*). Thalamic VAChT decrements, especially decrements in the right visual thalamus, were related to a history of falling. Freezing of gait correlated with lower VAChT in striatal interneurons and limbic cortices (*24*). In PD without dementia, dysfunction of memory, executive function, and attention correlated regionally with lower VAChT availability within the cingulate and insular cortices and thalamus (*25*). Sanchez-Catasus et al. determined striatal disbalance between acetylcholinergic and dopaminergic systems in mild to moderate PD using ^{18}F-FEOBV PET and other techniques (*26*). In cognitively normal PD patients, higher VAChT binding in the hippocampus, associated with cognitive measures, and lower VAChT binding in the posterior cortical regions were reported. Higher hippocampal VAChT binding in cognitively normal PD patients suggests a novel compensatory role for VAChT in PD (*27*). However, another potential cause for higher VAChT binding could be inflammatory changes, as demonstrated by ^{18}F-FEOBV PET in acute peripheral inflammation. More investigation, accounting for inflammatory changes, is required for VAChT PET studies of potential compensatory neuronal changes in neurodegenerative disorders (*28*).

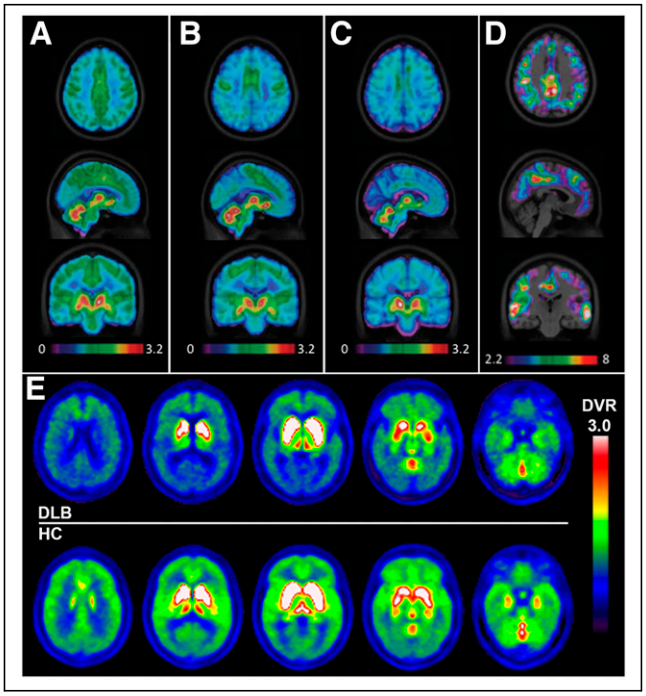

FIGURE 3. (A–D) ^{18}F-FEOBV VAChT binding (SUV ratio) using PET in 1 representative HC (A), mild-AD patient (B), and severe-AD patient (C) showing lower cortical VAChT binding depending on severity of AD. Statistical parametric analysis indicates significant clusters of lower cortical VAChT binding in AD compared with HC (D). (Modified with permission of (*17*).) (E) Another ^{18}F-FEOBV PET study demonstrating lower subcortical and cortical VAChT binding (SUV ratio) in 1 representative patient with LBD (top row) and 1 HC (bottom row). DVR = distribution volume ratio. (Reprinted with permission of (*18*).)

α4β2 nAChR

Structure, Distribution, and Function of α4β2 nAChRs

All nAChRs are pentameric. The heteromeric α4β2 subtype consists of α- and β-subunits, which form an ion channel (*29*). α4β2 nAChRs are ubiquitous in the human brain and are preferentially located at preterminal and presynaptic sites, acting as modulators of different neurotransmitters (*29*). The highest density of α4β2 nAChRs has been detected in the nucleus basalis of Meynert and the thalamus; density is moderate in the putamen and cerebellum and low in cortical regions (*30–32*). α4β2 nAChRs play an important role in higher cognitive processes such as learning and memory and are involved in addiction and depression (*31,33*). Postmortem studies reported a reduced α4β2 nAChR density in AD and LBD (*34–41*).

PET Radioligands for Imaging α4β2 nAChRs

Because of space restrictions, we will focus on the radiotracers most often used in preclinical and clinical research. Their chemical structures are summarized in Table 2 and Figure 2B. ^{11}C-nicotine was the first radiotracer used to image α4β2 nAChRs in vivo. Because the distribution of ^{11}C-nicotine was influenced by blood flow and blood–brain barrier transport, the estimated receptor densities were not reliable. This problem was overcome by the 3-pyridylether derivatives 2-^{18}F-FA-85380 and 6-^{18}F-FA-85380. However, these PET tracers suffer from slow kinetics. Nonetheless, both radioligands have been applied to investigate α4β2 nAChRs in vivo for many years. The next generation of PET radiotracers targeting α4β2 nAChRs, developed after the turn of the millennium, showed faster brain kinetics. This next generation contains 3 chemical classes. There are the advanced 3-pyridylether derivatives, such as ^{18}F-nifene; the derivatives of epibatidine,

TABLE 2
Most Relevant α4β2 nAChR PET Tracers

Tracer name	Formula
2-^{18}F-FA-85380	2-^{18}F-fluoro-3-(2(*S*)-azetidinylmethoxy)pyridine
6-^{18}F-FA-85380	6-^{18}F-fluoro-3-(2(*S*)-azetidinylmethoxy)pyridine
^{18}F-AZAN	(1*R*,2*R*,4*S*)-2-[5-(6-^{18}F-fluoranylpyridin-2-yl)pyridin-3-yl]-7-methyl-7-azabicyclo[2.2.1]heptane
^{18}F-XTRA	2-[5-[2-^{18}F-fluoropyridin-4-yl]pyridin-3-yl]-7-methyl-7-azabicyclo[2.2.1]heptane
(−)-^{18}F-flubatine	(−)-(1*R*,5*S*,6*S*)-6-(6-^{18}F-fluoropyridine-3-yl)-8-aza-bicyclo[3.2.1]octane
(+)-^{18}F-flubatine	(+)-(1*S*,5*R*,6*R*)-6-(6-^{18}F-fluoro-pyridine-3-yl)-8-aza-bicyclo[3.2.1]octane
^{18}F-nifene	3-[[(2*S*)-2,5-dihydro-1*H*-pyrrol-2-yl]methoxy]-2-^{18}F-fluoranylpyridine

such as ^{18}F-AZAN and ^{18}F-XTRA; and the derivatives of homoepibatidine, the enantiomers (−)-^{18}F-flubatine and (+)-^{18}F-flubatine. A scanning time of 40 min is sufficient for ^{18}F-nifene (*42*), whereas the other 4 radioligands require scans of at least 90 min (*43–47*). All radiotracers demonstrated a high affinity to their target structure (*42–47*). However, a difference can be observed considering the metabolization of these PET radioligands. The homoepibatidine derivatives show only a low level of metabolization in the case of (−)-^{18}F-flubatine and a negligible level in the case of (+)-^{18}F-flubatine (*44,45,47*). In contrast, the epibatidine derivatives ^{18}F-AZAN and ^{18}F-XTRA suffer from severe metabolization (*43,46*). Whether and to what amount ^{18}F-nifene is metabolized in humans has not been published, to the best of our knowledge.

For noninvasive quantitative modeling of α4β2 nAChR binding and to normalize for interindividual variability in α4β2 nAChR binding for between-group analyses, it is desired to have a receptor-free reference region. The human brain is most likely not fully free of α4β2 nAChRs. 2-^{18}F-FA-85380 PET studies revealed that α4β2 nAChR binding (distribution volume) in the corpus callosum is very low in nonsmokers but substantially higher in smokers (*48*). A 2-^{18}F-FA-85380 PET study was performed on smokers. Cigarette smoking to receptor satiety revealed that nicotinic receptor displacement in the corpus callosum was relatively low, at approximately 16% (*49*), and in a small (−)-^{18}F-flubatine PET study (n = 3) it was approximately 21% (*50*). This led to the assumption that α4β2 nAChR in the corpus callosum is negligible in nonsmokers but not in smokers. It was proposed that the distribution volume in the corpus callosum of nonsmokers may be similar to nondisplaceable binding and that the corpus callosum would be appropriate for use as a reference region (*48*). Thus, in 2-^{18}F-FA85380 or ^{18}F-flubatine PET studies, the corpus callosum was used as a reference region in nonsmoking patients with neurodegenerative disorders (*45,51,52*).

α4β2 nAChR Imaging Results in Neurodegeneration

Most PET imaging studies of α4β2 nAChRs in AD have been performed using 2-^{18}F-FA85380 PET. Clinical studies with the more recently developed second-generation α4β2 nAChR PET radioligands are limited to phase 0 and phase I data on (−)-^{18}F-flubatine and (+)-^{18}F-flubatine. Regarding AD, the conducted PET studies could confirm a reduction in cerebral α4β2 nAChRs in regions typically affected by AD, such as the temporal, mesiotemporal, frontal, prefrontal, and parietal cortices, as well as in subcortical areas such as the caudate nucleus and thalamus (*45,47,51–54*).

Different study groups also investigated the correlations between cognitive performance and availability of cerebral α4β2 nAChRs in AD. Two 2-^{18}F-FA-85380 studies showed significant correlations of the caudate nucleus and the frontal, temporal, anterior, and posterior cingulate cortices with global cognitive scores such as the mini mental state examination, DemTect, or clock-drawing test scores (*51,52*). Another 2-^{18}F-FA-85380 PET study reported a moderate to strong correlation between the frontal assessment battery and the mesiotemporal cortex and basal forebrain (*53*).

In the (−)-^{18}F-flubatine PET study on mild AD dementia, using volume-of-interest–based regression analysis, executive function showed an association with α4β2 nAChR availability in the frontal and parietal brain regions, and episodic memory showed an association with availability in the frontal, mesiotemporal, and parietal cortices. More interestingly, in AD, explorative voxel-based regression analysis revealed a highly significant association between memory and α4β2 nAChR availability in the basal forebrain (Fig. 4) (*45*).

In PD and DLB, in vivo examination and investigation of α4β2 nAChRs were performed mainly with 5-^{123}I-IA85380 SPECT and 2-^{18}F-FA-85380 PET. These studies consisted of small to moderately sized groups and showed reduced α4β2 nAChRs in the thalamus, caudate nucleus, substantia nigra, and different cortical regions in DLB and PD patients (*55–58*).

Using 2-^{18}F-FA-85380 PET in PD patients with an additional depressive syndrome or a mild cognitive impairment, the alterations were more pronounced (*58*). Using 5-^{123}I-IA85380 SPECT, the association between cognitive performance and α4β2 nAChR availability was confirmed by a further study on 25 nondemented patients with PD (*59*). Two 5-^{123}I-IA85380 SPECT studies reported that increased α4β2 nAChRs in the occipital cortex were observed in DLB with visual hallucinations (*56*) and in early PD in brain regions of the motor and limbic basal ganglia circuits (*60*).

α7 α4β2 nAChR

Structure, Distribution, and Function of α7 nAChRs

α7 nAChRs represent the second most abundant nAChR subtype in the human brain. They are expressed by many brain cell types, such as neurons, astrocytes, microglia, oligodendrocyte precursor cells, and endothelial cells. As such, α7 nAChRs are widely distributed throughout the human brain, with density being highest in the thalamus, hippocampus, and basal forebrain (*61*). Regarding its nonneuronal expression, α7 nAChR acts as an essential regulator of inflammation (*62*).

The affinity of α7 nAChR to agonists such as nicotine or acetylcholine is low, whereas that to the antagonist α-bungarotoxin is high. A special feature of α7 nAChR is its high permeability for

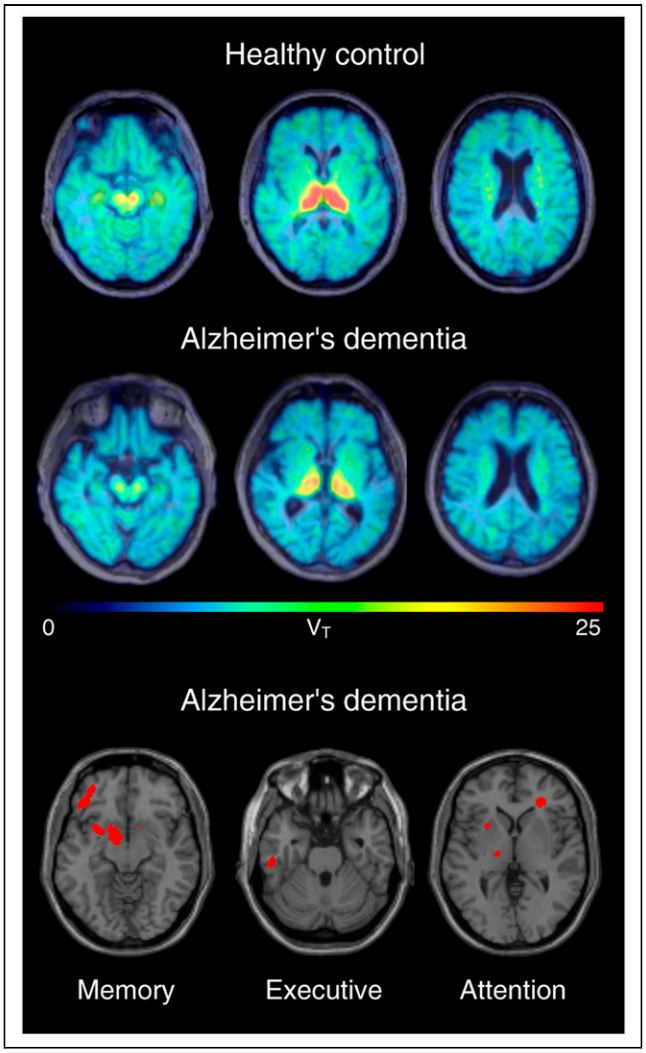

FIGURE 4. (−)-^{18}F-flubatine PET showed lower cortical α4β2 nAChR (α4β2 nAChR) availability (distribution volume [V_T] parametric images) in mild AD (middle row) than in HCs (top row). In AD, there were relevant associations between networks of disturbed subcortical and cortical α4β2 nAChR binding and dysfunction of episodic memory, executive/working memory, and attention (bottom row). (Modified from (*45*).)

Ca^{2+} ions (*63*), rendering it a calcium channel. Via its influence on the Ca^{2+} balance, α7 nAChRs influence different neurotransmitters, receptors, cell survival, brain plasticity and gene expression. Thus, under physiologic conditions, the action of α7 nAChRs influences memory, development, attention, and other processes.

α7 nAChRs in Neurodegeneration

In several neurodegenerative diseases, this α7 nAChR action is altered. In the late-stage human AD brain, for instance, α7 nAChR protein levels are reduced in certain areas (*64*). In contrast, increased levels of α7 nAChR protein were reported in early AD stages (*65*). Of note, β-amyloid has picomolar—that is, very high—affinity to α7 nAChR (*66*). In advanced AD, the larger amyloid burden seems to block α7 nAChRs, possibly promoting, at least in part, cognitive breakdown (*67*). It is also known that binding of soluble β-amyloid to α7 nAChRs can promote intraneuronal amyloid accumulation and tau phosphorylation (*68*). Altogether, there is a direct, although complex, relationship between neurodegeneration, neuroinflammation, and α7 nAChR expression.

PET Radioligands for Imaging α7 nAChRs

Here, we will give an overview of the most interesting α7 nAChR PET tracers that have been developed over the years. Details on these tracers are provided in Table 3 and Figure 2C.

The search for suitable α7 nAChR PET tracers faces some challenges: the density of these receptors in the human brain is lower than that of the abundant α4β2 nAChRs. Also, there is high structural similarity between α7 nAChR and another member of the ligand-gated ion channel superfamily, the 5-hydroxytryptamine-3 receptor.

Most α7 nAChR PET tracers of interest are diazabicyclononane derivatives. Of this group, ^{11}C-CHIBA-1001 was the first entering human application (*69,70*). However, subsequent research reported limited binding affinity, limited binding selectivity, and inadequate brain distribution for this tracer (*71*). Also, a series of diazabicyclononane derivatives possessing sufficient brain uptake was developed (^{11}C-NS14492, ^{18}F-NS10743, and ^{18}F-NS14490). However, observation of specific brain binding in preclinical research was limited (*72*). Other candidates are the dibenzothiophene sulfone derivative ^{18}F-ASEM and its paraisomer ^{18}F-DBT10. Both tracers yielded satisfying and similar brain kinetics in nonhuman primates, as well as significant specific binding in the human brain (*71*). For ^{18}F-ASEM applied to HCs of a considerable age range, regional ^{18}F-ASEM binding correlated positively with age (*73*).

As an alternative α7 nAChR PET tracer, the azabicyclooctylester ^{11}C-MeQAA was developed. Although specific in vitro binding was demonstrated for this tracer, in vivo selectivity was limited by

TABLE 3
Most Relevant α7 nAChR PET Tracers

Tracer name	Formula
^{11}C-CHIBA-1001	4-^{11}C-methylphenyl)-1,4-diazabicyclo[3.2.2]nonane-4-carboxylate
^{11}C-NS14492	(2-(1,4-diazabicyclo[3.2.2]nonan-4-yl)-5-(1-^{11}C-methyl-1*H*-pyrrol-2-yl)-1,3,4-oxadiazole)
^{18}F-NS10743	2-(1,4-diazabicyclo[3.2.2]nonan-4-yl)-5-(4-^{18}F-fluorophenyl)-1,3,4-oxadiazole
^{18}F-NS14490	(1*R*,5*S*)-3-(6-(1-(2-^{18}F-fluoroethyl)indol-5-yl)pyridazin-3-yl)-9-methyl-3,9-diazabicyclo[3.3.1]nonane
^{18}F-DBT10	7-(1,4-diazabicyclo[3.2.2]nonan-4-yl)-2-^{18}F-fluorodibenzo[*b,d*]thiophene 5,5-dioxide
^{18}F-ASEM	7-(1,4-diazabicyclo[3.2.2]nonan-4-yl)-4-^{18}F-fluorodibenzo[*b,d*]thiophene 5,5-dioxide
^{11}C-MeQAA	(1*S*,3*R*,4*S*)-quinuclidin-3-yl 3-(^{11}C-methylamino)benzoate

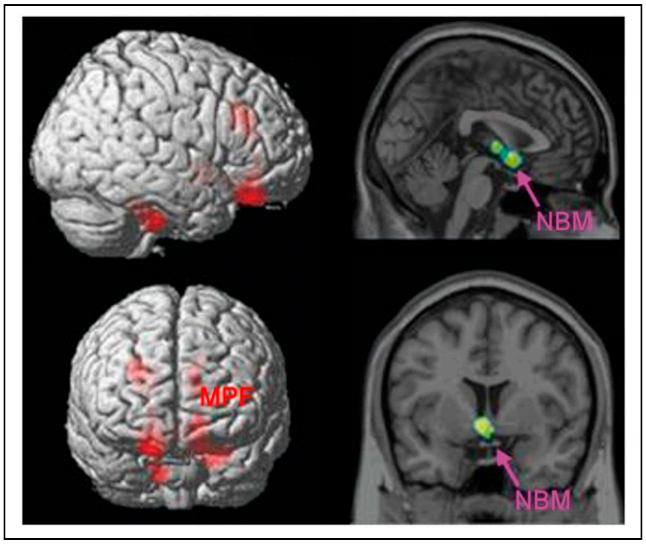

FIGURE 5. Statistical parametric mapping–based correlations between ^{11}C-MeQAA α7 nAChR binding as assessed by PET imaging and frontal-assessment-battery scores in patients with AD. MPF = medial prefrontal cortex; NBM = nucleus basalis of Meynert. (Reprinted with permission of (*76*).)

concomitant off-target binding to 5-hydroxytryptamine-3 receptors (*74,75*).

α7 nAChR Imaging Results in Neurodegeneration

So far, 2 α7 nAChR PET imaging studies in human neurodegenerative disorders have been published: Nakaizumi et al. (2018) applied ^{11}C-MeQAA α7 nAChR and ^{11}C-Pittsburgh compound B amyloid PET imaging to 20 patients with clinically diagnosed AD and to 10 age-matched HCs (*76*). In this study, the specific ^{11}C-MeQAA binding was significantly lower in AD than in HCs in the temporal and prefrontal brain areas. Further, there was a correlation between the ^{11}C-MeQAA uptake in the basal cholinergic forebrain region and frontal cognition deficits in AD (Fig. 5) (*76*). In another study, Coughlin et al. (2020) compared the specific brain binding of ^{18}F-ASEM in subjects with the potential prodromal AD stage of mild cognitive impairment with that in HCs. Higher uptake in the brain was observed for the mild cognitive impairment cohort (*77*). These initial human α7 nAChR PET data encourage expansion to other neurodegenerative disorders and other AD disease stages, thereby allowing gathering of more insight into potential future applications for this novel PET technology.

mAChR

Structure, Distribution, and Function of mAChRs

The structure of mAChRs is completely different from that of nAChRs. They belong to the metabotropic G-protein–coupled receptors. Similar to nAChRs, the distribution of mAChRs is widespread in the human brain and mAChRs act as modulators of neuronal activity (*78*). The highest density of mAChRs is in the occipital and insular cortices and the basal ganglia. The thalamus and cerebellum possess only low and very low amounts of mAChRs, respectively (*79*). The 5 subtypes (M1–M5) divide into 2 classes. The M1 receptor class comprises the subtypes M1, M3, and M5, which are $G_{q/11}$ G-protein–coupled, whereas the M2 receptor class includes the M2 and M4 subtypes, which signal through $G_{i/o}$ G-proteins (*80,81*). In general, the subtypes M1, M3, and M5 are usually postsynaptically located and increase the excitatory effects of transmitters, whereas M2 and M4 display the main presynaptic mAChRs and have an inhibitory action by suppressing transmitter release (*81*).

In the human brain, M1, M2, and M4 mAChRs are the most frequent subtypes (*81*), whereas M1 and M4 are the most abundant, though M1 mAChRs are relatively higher in the cortex (35%–60%) and M4 mAChRs are relatively higher in the striatum, especially in the putamen (!50%) (*81*). The M2 mAChRs are the predominant subtype in the basal forebrain (!40%) and thalamus (*81*).

In consolidation of memory and in higher brain functions such as cortex-dependent processing and cortex–hippocampus interactions, the postsynaptic and predominantly cortically located M1 mAChR subtype plays an important role (*78,81*).

mAChRs in Neurodegeneration

Several histopathology studies using unselective mAChR radioligands showed lower mAChRs binding in the human brain in AD and PD (*79*).

In transgenic AD mouse models, the additional knockout of M1 mAChRs results in a severely increased AD pathology (*78*), supporting the assumption that M1 mAChRs seem to be an important regulator of amyloidogenesis and a therapeutic target for AD. Postmortem data from AD patients revealed a normal density of M1 mAChRs (*82,83*). A further recently published postmortem study hypothesized that the cholinergic dysfunction of M1 mAChRs might be associated with an activation of the glutamate receptor 5 (mGluR5) due to β-amyloid (*84*). Because both M1 mAChRs and mGluR5 use the same $G_{q/11}$ G-protein–coupled signal pathway, an increased activation of mGlu5R might result in a reduced availability of the G-proteins for the M1 mAChR (*84*). Another hypothesis is that β-amyloid itself destabilizes the M1/G-protein coupling (*84*). In the pathophysiologic process of PD, the M1 mAChRs seem to be of relevance, too. Two preclinical studies on rodents found an improvement in PD motor symptoms after blocking of M1 mAChRs on striatal neurons (*85,86*).

The knockout of M2 mAChR in mice resulted in an impairment of higher cognitive functions such as working memory, spatial learning, and behavioral flexibility (*78*). Overall, data on M2 mAChR in neurodegenerative diseases are limited. Two postmortem studies detected reduced presynaptic M2 mAChRs in cortical regions in AD patients (*87,88*). It is hypothesized that the loss of M2 mAChRs in AD begins in the late stage of mild cognitive impairment and progresses during the course of the disease (*81*).

M4 mAChRs are the predominant subtype in the striatum (*81*). M4 mAChR knockout mice showed unimpaired episodic memory and orientation but decreased anxiety (*78*). Moreover, in animal models, positive allosteric activators of M4 could decrease dopamine release and demonstrate antipsychotic effects (*89*). In contrast, blocking of postsynaptic M4 mAChRs on striatal medium spiny neurons seems to reduce motor symptoms in preclinical PD models (*85,86*). In a postmortem study of patients with moderate to severe PD, an upregulation of M2 and M4 mAChRs was demonstrated in the dorsolateral and mesioprefrontal cortices (*90*). The authors hypothesized a compensation for the loss of cholinergic innervation. In AD, 1 study showed an increase in immunoprecipitated M4 mAChRs in the frontal, temporal, and parietal cortices (*82*).

PET Radioligands for Imaging mAChRs

The development of PET radioligands to image mAChRs has a long history beginning in the late 1970s (*79,91*). As with the

TABLE 4
Most Relevant mAChR PET Tracers

Tracer name	Formula	Selectivity
^{18}F-FP-TZTP	3-(4-(3-^{18}F-fluoropropylthio)-1,2,5-thiadiazol-3-yl)-1-methyl-1,2,5,6-tetrahydropyridine	M2 (M1)*
^{11}C-LSN3172176	Ethyl-4-(6-(methyl-^{11}C)-2-oxoindolin-1-yl)-[1,4′-bipiperidine]-1′-carboxylate	M1
^{11}C-MK-6884	6-(2-methyl-3-oxoisoindolin-5-yl)-5-(1-((1-methylcyclopentyl)methyl)-1*H*-pyrazol-4-yl)picolinonitrile	M4

*Lower affinity as well reported for M1 (*91*).
Methodologic determination of selectivity was previously published (*91*).

nAChR-targeting radioligands, the first radiotracers developed to image mAChRs suffered from insufficient subtype selectivity and unfavorable tracer kinetics, resulting in complicated modeling analyses (*79,91*). The development of subtype-specific radiotracers is still a work in progress (*91*). There are promising candidates for imaging M1, M2, and M4 mAChRs (Table 4; Fig. 2D). ^{11}C-LSN3172176 is a novel M1-selective mAChR PET radiotracer. In the first-in-humans study, a scan duration of 80 min was sufficient for quantification of M1 mAChR by 1-tissue-compartment modeling or by the noninvasive simplified reference tissue model 2, and the metabolization was classified as moderate (Fig. 6) (*92*). For imaging M2 mAChR, the PET radiotracer ^{18}F-FP-TZTP showed encouraging results in preclinical and clinical studies (*93,94*). A scanning duration of 120 min is sufficient, and quantification is possible by using a 2-parameter multilinear reference tissue model (*95*). The M1-selective mAChR PET ligand ^{11}C-GSK1034702 has recently been translated to clinical application using PET (*91*). Tracer development and clinical PET application of ^{11}C-GSK1034702 was proposed to assess blood–brain barrier permeability and to lower the risk of the drug development process for GSK1034702. However, because of limited specific binding as a result of low affinity to the target, it was concluded that ^{11}C-GSK1034702 is not a suitable PET ligand (*91*). A recently published study described the synthesis of, and preclinical data on, a novel ^{11}C-labeled positive allosteric modulator of M4 mAChR named ^{11}C-MK-6884 (*96*). In rhesus monkeys, the radioligand showed rapid penetration of the blood–brain barrier, a local distribution pattern in the CNS similar to the known pattern for M4 mAChR (i.e., highest in the striatum), and a high receptor occupancy of 87%. This PET ligand binds with high affinity and good selectivity to an allosteric site on M4 mAChR. It was shown that ^{11}C-MK-6884 binds to activated M4 mAChR, a finding that agrees with its pharmacology as a highly cooperative positive allosteric modulator of M4 (*96,97*). ^{11}C-MK-6884 was recently translated to clinical PET application (*96,97*). The first-in-humans application of the nonselective mAChR PET ligand 4-^{18}F-fluorodexetimide showed promising findings, including high brain uptake, high image quality, unspecific binding in the cerebellum (making it valid to be used as a reference region), low interindividual variability in healthy subjects, and irreversible kinetics of tracer distribution in brain regions high in mAChRs (*98*). The nonselective M1 and M4 SPECT ligand ^{123}I-iodoquinuclidinylbenzilate, in combined use with ^{99m}Tc-exametazime SPECT to account for cerebral blood flow, is successfully used for cholinergic receptor network investigations on neurodegenerative disorders (*99*).

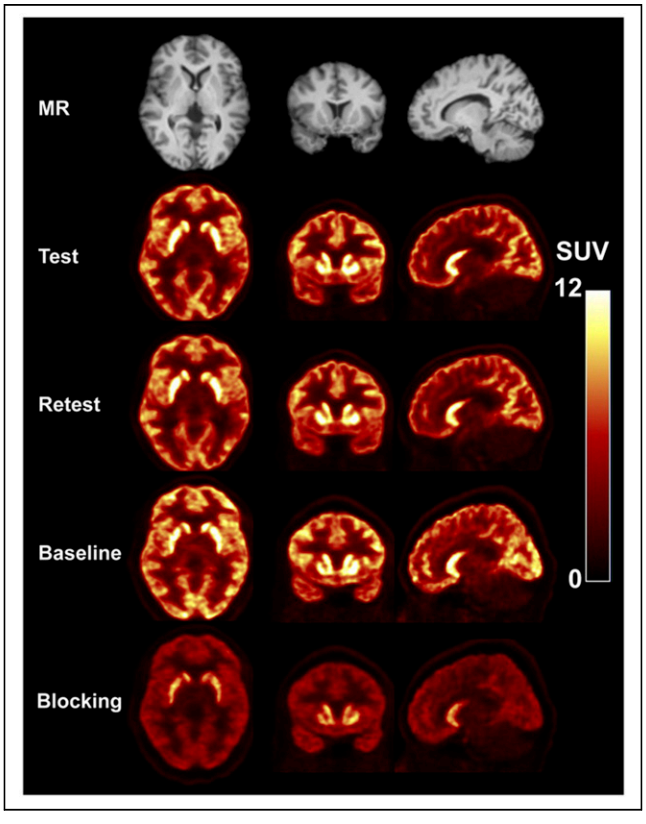

FIGURE 6. First-in-humans PET study on healthy subjects using M1 mAChR radioligand ^{11}C-LSN3172176 showing high reproducibility under test–retest conditions and relevant blocking effects between baseline and blocking state using mAChR antagonist scopolamine. Cerebellum is potentially mAChR-free and can be used as reference region. (Reprinted from (*92*).)

mAChR Imaging Results in Neurodegeneration

The nonselective SPECT ligand ^{123}I-iodoquinuclidinylbenzilate targeting M1 and M4 mAChRs has been successfully used for novel important network analyses of mAChR modulatory contributions to large-scale alterations in brain-network function in AD and DLB (*99,100*).

M1- and M2-selective mAChR PET imaging studies on patients with neurodegenerative diseases are still pending, despite the promising first clinical data on the M1 mAChR–selective radioligand ^{11}C-LSN3172176 and the availability of the M2 mAChR–selective radioligand ^{18}F-FP-TZTP. The first-in-humans PET investigation of the M4 mAChR–selective PET ligand ^{11}C-MK-6884 was performed in AD and HCs (*97*). In moderate to severe AD, compared with HCs, there was lower M4 mAChR binding in the

frontal and temporal cortices. In contrast, M4 mAChR binding in the striatum did not differ between groups. PET imaging of M1-, M2-, or M4-selective mAChRs is especially interesting to assess receptor occupancy by M1, M2, or M4 mAChR drugs or receptor activation by other cholinergic drugs such as AChE inhibitors, improving drug development in neurodegenerative disorders.

ACETYLCHOLINESTERASE

Local Distribution of AChE

In the human brain, AChE activity is highest in the striatum, followed by the basal forebrain, cerebellum, thalamus, brain stem, and cerebral cortex (*101–103*). The distribution of AChE in the CNS conforms widely to the distribution of choline acetyltransferase (*104*). AChE is located in presynaptic, intrasynaptic, and, to a lesser extent, postsynaptic neurons and in noncholinergic and cholinoceptive neurons. Although AChE is not so pure a preterminal cholinergic measure as choline acetyltransferase or VAChT, assessment of AChE activity is regarded as a reliable biomarker of the cholinergic system in the CNS (*102,103*).

PET Radioligands for Imaging AChE Activity

Two different classes of PET tracers were developed to assess AChE activity in the brain: the first is AChE inhibitors, such as ^{11}C-physostigmine or 5-^{11}C-methoxy-donepezil (*102,103*), and the second is substrates of ACh. The PET radioligands ^{11}C-methylpiperidin-4-yl propionate (^{11}C-PMP) and *N*-^{11}C-methylpiperidinyl-4-acetate (^{11}C-MP4A) are analogs of acetylcholine (Table 5; Fig. 2E). They are hydrolyzed by AChE, and their hydrophilic metabolite *N*-^{11}C-methyl-piperidinol is irreversibly trapped within the brain. Compared with ^{11}C-PMP, ^{11}C-MP4A is slightly more selective for AChE (*105*) but possesses a higher relative hydrolysis rate (k_3) and is more flow-limited. Thus, ^{11}C-PMP discriminates better between distinct AChE brain regions than does ^{11}C-MP4A. ^{11}C-PMP provides accurate measures of cortical and thalamic AChE, whereas ^{11}C-MP4A gives precise measures of cortical AChE. Very high availability of striatal AChE and limitation of delivery restrict precise assessment of striatal AChE for both tracers (*102,103,105*). Both tracers were validated and sensitive enough to detect a 30%–50% decrease in AChE activity in an experimental AD model (*102,105,106*). Using AChE PET, there was no age-related decline of cerebral AChE activity in HCs (*107,108*). Using AChE PET in HCs, AChE activity was highest within the striatum, followed by the cerebellar cortex, thalamus, and cerebral cortex, paralleling the physiologic distribution of AChE activity in postmortem human brain (*101,108*). In HCs, AChE activity was sufficiently blocked by the AChE inhibitor physostigmine in the temporal cortex (49%) (*108*).

AChE Imaging Results in Neurodegeneration

The first AChE PET investigations in AD, using ^{11}C-MP4A or ^{11}C-PMP PET, were performed in the late 1990s. Cholinergic dysfunction in neurodegenerative diseases using AChE PET has extensively been studied since then. Because of space restrictions, only a limited number of PET studies can be covered. Excellent recent reviews are recommended for further reading (*103,109,110*). As found by ^{11}C-MP4A PET, cortical AChE activity was reduced by a maximum in the parietal (−38%) and temporal cortices (−31%), compared with HCs (*111*). Using ^{11}C-PMP PET, cortical AChE activity, especially in the temporal cortex, was lower in AD than in HCs (−30%). The pattern of lower cortical AChE activity in AD was similar to the pattern of decreased VAChT binding but distinct from glucose metabolism (*108*). Shinotoh et al. demonstrated a progressive decline in cortical AChE activity in AD in a longitudinal study (2-y follow-up) and a relationship between lower cortical AChE activity and global cognitive dysfunction. Compared with HCs, EOAD showed lower cortical and hippocampal AChE activity than did LOAD (Fig. 7A and 7B) (*103,112*). Rinne et al. demonstrated a modest decline in hippocampal AChE activity in amnestic mild cognitive impairment (−17%) and early AD (−27%) (*113*). Similarly, in mild to moderate AD a modest decline in cortical AChE binding (−11%) was reported that correlated

TABLE 5
Most Relevant AChE PET Radioligands

Tracer name	Formula
^{11}C-MP4A	*N*-^{11}C-methylpiperidyl acetate
^{11}C-PMP	*N*-^{11}C-methylpiperidyl propionate
^{11}C-donepezil	5-^{11}C-methoxy-donepezil

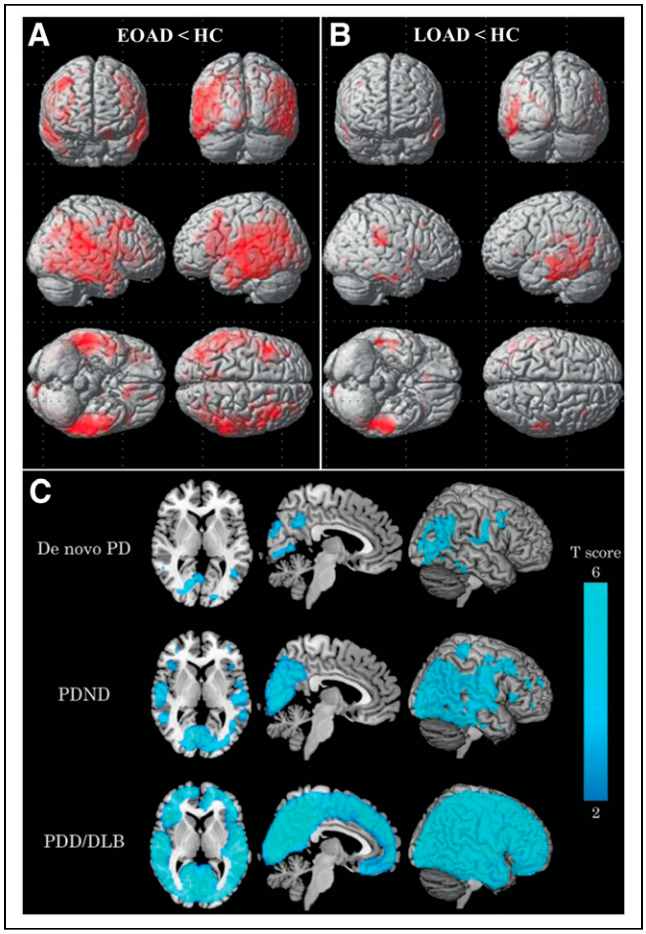

FIGURE 7. (A) As assessed by ^{11}C-MP4A PET, compared with HCs there is lower AChE binding in temporoparietal cortices in EOAD. (B) However, in LOAD, decreased AChE binding is restricted to temporal cortices. (C) Using ^{11}C-MP4A PET, various stages of LBD were investigated and compared with HCs. There is lower AChE binding in medial occipital cortex in de novo PD. There is reduced cortical AChE binding in PD without dementia (PDND). Most widespread cortical AChE decrease is in PDD or DLB, not differing from each other. (Reprinted with permission of (*103*).)

especially with disturbed attention and working memory but less with primary memory (*114*). Using ^{11}C-PMP PET in AD, a clinical dose of the AChE inhibitor donepezil demonstrated minor inhibition of AChE activity (−27%) (*115*). This finding was supported by AChE PET studies using various AChE inhibitors reporting modest blocking of AChE activity by 20%–40% (*103*). Recently, an elegant placebo-controlled ^{11}C-MP4A PET/functional MRI study using the AChE inhibitor rivastigmine was performed on patients with early AD and HCs. The authors demonstrated that lower cortical and rather preserved hippocampal AChE activity in early AD are prognostic for the memory response to rivastigmine (*116*).

Using ^{11}C-PMP PET in atypical parkinsonian syndromes, such as multiple-system atrophy and progressive supranuclear palsy, subcortical AChE activity was more reduced than in PD. Lower AChE activity in the brain stem and cerebellum correlated with disturbances in gait and balance. The important findings potentially reflect greater dysfunction of the pontine cholinergic system, which is relevant for motor function, such as gait, in atypical parkinsonian syndromes (*117*).

An ^{11}C-MP4A PET study performed by the Chiba group in 1999 investigated AChE activity in PD and progressive supranuclear palsy. Compared with HCs, PD patients showed the lowest cortical AChE activity (−17%) and progressive-supranuclear-palsy patients showed the lowest thalamic AChE activity (−38%). Different patterns of cholinergic dysfunction proposed a potential role for AChE PET in differential diagnosis between PD and progressive supranuclear palsy (*103*). In LBD patients, compared with HCs, there was lower cortical AChE activity, especially in the medial occipital cortex in early PD. Widespread, and the largest, reduction in AChE activity was found in PDD and DLB, not differing from each other (Fig. 6C) (*103*). Using ^{11}C-PMP PET, compared with HCs, cortical AChE activity was lowest in PDD (−20%), followed by PD (−13%) and mild LOAD (−9%). Mild LOAD showed the lowest AChE activity within the temporal cortex (−15%) (*118*). In PD and PDD, there was the most significant relationship between lower cortical AChE activity and attentional and executive dysfunction (*119*).

More recently, there has been increasing interest in using AChE PET for investigation of associations between cholinergic dysfunction and noncognitive symptoms such as gait problems and falls, neuropsychiatric symptoms, olfactory dysfunction, and sleep problems in PD (*109,111*).

Bohnen et al. found that the decrease in brain stem–thalamic AChE activity was more related to the fall status in PD than to the decline in cortical AChE binding and was not related to nigrostriatal dopamine loss (*109*). Interestingly, most of these PD patients with lower thalamic AChE binding also had decreased cortical AChE activity. The Michigan group found that in PD with freezing of gait symptoms, the decline in cortical AChE activity was more pronounced than the decreased thalamic AChE binding. In PD, lower cortical AChE binding was related to a slower gait speed. In PD, lower thalamic AChE activity correlated with dysfunctional sensory processing while under postural control (*109*). Thus, gait and balance dysfunction in PD is possibly the result of a complex interrelationship between multiple dysfunctional systems and neurotransmitters, including degeneration of the cholinergic basal forebrain and the brain stem (*109,110*).

Importantly, higher AChE activity was reported in carriers of LRRK2 mutations in premanifest and manifest PD and may reflect compensatory changes (*120*). However, higher AChE activity may also be a result of inflammation, as shown in preclinical and clinical studies of peripheral inflammation using ^{11}C-donepezil PET (*28*). More investigations, using both cholinergic and specific inflammation PET ligands in the same PD patients, are needed in future trials.

Importantly, recent reports of α-synucleinopathy in the body and brain in LBD and cholinergic dysfunction in the body in early or prodromal LBD, such as the gut, as determined by ^{11}C-donepezil PET, led to a paradigm shift regarding our understanding of the pathophysiology of LBD and established the definition of the body-first versus brain-first LBD subtypes (*7,8*).

CONCLUSIONS AND FUTURE DIRECTIONS

The possibility of obtaining in vivo information about the integrity of cholinergic transmission by means of PET imaging is of major interest in studying neurodegenerative disorders. This option refers to all the different compartments of this complex neurotransmitter system.

The development and successful clinical translation of ^{18}F-FEOBV was a breakthrough for PET imaging of VAChT binding in the human brain. Recently, the number of ^{18}F-FEOBV PET studies on AD and LBD has rapidly increased. The study findings are exciting, provide novel information on VAChT pathophysiology, and may lead to novel paradigms for cholinergic drug therapy in LBD.

Several α4β2 nAChR–targeting tracers have been developed, with the recent-generation tracers ^{18}F-AZAN, ^{18}F-XTRA, ^{18}F-nifene, (−)-^{18}F-flubatine, and (+)-^{18}F-flubatine possessing favorable imaging characteristics. The highest potential for PET imaging of α4β2 nAChRs seems to be in monitoring disease progression and the respective therapies.

Only recently has it become possible to image α7 nAChR availability in the human brain in vivo by PET using ^{18}F-ASEM or ^{11}C-MeQAA. α7 nAChRs have a complex behavior and represent an interesting diagnostic and therapeutic target in neurodegenerative disorders because the brain availability of α7 nAChRs in these disorders is a function of disease stage as well as degree of neurodegeneration and neuroinflammation. Of special note for AD imaging, β-amyloid interferes with α7 nAChRs in a concentration-dependent manner. As such, α7 nAChR PET imaging is seen as the most promising for disease staging, progression estimation, and drug testing in neurodegenerative disorders.

The development of selective mAChR PET ligands is important but difficult. There are promising findings from first-in-humans PET applications using the M1 mAChR–selective ligand ^{11}C-LSN3172176 and the M4 mAChR–selective ligand ^{11}C-MK-6884. The M2 mAChR–selective ligand ^{18}F-FP-TZTP is established. First-in-humans application of the nonselective mAChR PET ligand 4-^{18}F-fluorodexetimide showed promising results.

PET imaging of AChE activity has a long history. ^{11}C-PMP or ^{11}C-MP4A PET ligands were extensively used to assess lower cortical AChE availability in dementia associated with neurodegenerative diseases such as AD and LBD. More recently, novel findings in LBD (PD, PDD, and DLB) showed the relationship between lower cortical and subcortical cholinergic (AChE) binding and noncognitive dysfunctions such as balance and gait, wake/sleep cycle, olfaction, and mood in LBD. AChE inhibitors are one of the only two approved drug groups to treat AD, PDD, and DLB.

Higher AChE and VAChT binding in LRRK2 mutation carriers of manifest and premanifest PD and early PD may be a result of compensation or inflammation. The use of novel network analyses of cholinergic receptors in AD and LBD enables us to understand

the cholinergic modulatory contributions to large-scale network functions. The findings of cholinergic PET in the body, such as the gut, in early or prodromal PD contributed to a paradigm shift in our understanding of the pathophysiology of LBD and established the concept of a body-first and brain-first subtype of LBD.

Taken together, molecular imaging of different compartments of cholinergic neurotransmission is of great interest in different neurodegenerative disorders. For many aspects of cholinergic transmission, suitable tracers are available, with more to come. They will broaden our research application portfolio and potentially gain relevance in clinical care, such as by promoting the use of personalized medicine to guide cholinergic treatment decisions.

DISCLOSURE

No potential conflict of interest relevant to this article was reported.

REFERENCES

1. Mufson EJ, Ginsberg SD, Ikonomovic MD, DeKosky ST. Human cholinergic basal forebrain: chemoanatomy and neurologic dysfunction. *J Chem Neuroanat.* 2003;26:233–242.
2. Fisher SK, Wonnacott S. Acetylcholine. In: Brady ST, Siegel GJ, Albers RW, Price DL, eds. *Basic Neurochemistry.* 8th ed. Academic Press; 2012:258–282.
3. Hampel H, Mesulam M-M, Cuello AC, et al. The cholinergic system in the pathophysiology and treatment of Alzheimer's disease. *Brain.* 2018;141:1917–1933.
4. Bohnen NI, Albin RL. The cholinergic system and Parkinson disease. *Behav Brain Res.* 2011;221:564–573.
5. Bartus RT, Dean RL III, Beer B, Lippa AS. The cholinergic hypothesis of geriatric memory dysfunction. *Science.* 1982;217:408–414.
6. Christensen H, Maltby N, Jorm AF, Creasey H, Broe GA. Cholinergic 'blockade' as a model of the cognitive deficits in Alzheimer's disease. *Brain.* 1992;115: 1681–1699.
7. Fedorova TD, Seidelin LB, Knudsen K, et al. Decreased intestinal acetylcholinesterase in early Parkinson disease: an ^{11}C-donepezil PET study. *Neurology.* 2017; 88:775–781.
8. Borghammer P, Horsager J, Andersen K, et al. Neuropathological evidence of body-first vs. brain-first Lewy body disease. *Neurobiol Dis.* 2021;161:105557.
9. Wenzel B, Deuther-Conrad W, Scheunemann M, Brust P. Radioligand development for PET imaging of the vesicular acetylcholine transporter (VAChT) in the brain. In: Dierckx RA, Otte A, de Vries EF, van Waarde A, Lammertsma AA, eds. *PET and SPECT of Neurobiological Systems.* Springer International Publishing; 2021:1061–1090.
10. Jung YW, Frey KA, Mulholland GK, et al. Vesamicol receptor mapping of brain cholinergic neurons with radioiodine-labeled positional isomers of benzovesamicol. *J Med Chem.* 1996;39:3331–3342.
11. Kuhl DE, Koeppe RA, Fessler JA, et al. In vivo mapping of cholinergic neurons in the human brain using SPECT and IBVM. *J Nucl Med.* 1994;35:405–410.
12. Mulholland GK, Wieland DM, Kilbourn MR, et al. [^{18}F]fluoroethoxy-benzovesamicol, a PET radiotracer for the vesicular acetylcholine transporter and cholinergic synapses. *Synapse.* 1998;30:263–274.
13. Kilbourn MR, Hockley B, Lee L, et al. Positron emission tomography imaging of (2R,3R)-5-[(^{18})F]fluoroethoxybenzovesamicol in rat and monkey brain: a radioligand for the vesicular acetylcholine transporter. *Nucl Med Biol.* 2009;36:489–493.
14. Parent MJ, Bedard MA, Aliaga A, et al. Cholinergic depletion in Alzheimer's disease shown by [^{18}F]FEOBV autoradiography. *Int J Mol Imaging.* 2013;2013: 205045.
15. Petrou M, Frey KA, Kilbourn MR, et al. In vivo imaging of human cholinergic nerve terminals with (−)-5-^{18}F-fluoroethoxybenzovesamicol: biodistribution, dosimetry, and tracer kinetic analyses. *J Nucl Med.* 2014;55:396–404.
16. Albin RL, Bohnen NI, Muller MLTM, et al. Regional vesicular acetylcholine transporter distribution in human brain: a [^{18}F]fluoroethoxybenzovesamicol positron emission tomography study. *J Comp Neurol.* 2018;526:2884–2897.
17. Aghourian M, Legault-Denis C, Soucy JP, et al. Quantification of brain cholinergic denervation in Alzheimer's disease using PET imaging with [^{18}F]-FEOBV. *Mol Psychiatry.* 2017;22:1531–1538.
18. Nejad-Davarani S, Koeppe RA, Albin RL, Frey KA, Müller MLTM, Bohnen NI. Quantification of brain cholinergic denervation in dementia with Lewy bodies using PET imaging with [^{18}F]-FEOBV. *Mol Psychiatry.* 2019;24:322–327.
19. Jin H, Yue X, Liu H, et al. Kinetic modeling of [^{18}F]VAT, a novel radioligand for positron emission tomography imaging vesicular acetylcholine transporter in nonhuman primate brain. *J Neurochem.* 2018;144:791–804.
20. Liang Q, Joshi S, Liu H, et al. In vitro characterization of [^{3}H]VAT in cells, animal and human brain tissues for vesicular acetylcholine transporter. *Eur J Pharmacol.* 2021;911:174556.
21. Kuhl DE, Minoshima S, Fessler JA, et al. In vivo mapping of cholinergic terminals in normal aging, Alzheimer's disease, and Parkinson's disease. *Ann Neurol.* 1996;40:399–410.
22. Liu AK, Chang RC, Pearce RK, Gentleman SM. Nucleus basalis of Meynert revisited: anatomy, history and differential involvement in Alzheimer's and Parkinson's disease. *Acta Neuropathol (Berl).* 2015;129:527–540.
23. Mazère J, Lamare F, Allard M, Fernandez P, Mayo W. ^{123}I-iodobenzovesamicol SPECT imaging of cholinergic systems in dementia with Lewy bodies. *J Nucl Med.* 2017;58:123–128.
24. Bohnen NI, Kanel P, Zhou Z, et al. Cholinergic system changes of falls and freezing of gait in Parkinson's disease. *Ann Neurol.* 2019;85:538–549.
25. van der Zee S, Müller MLTM, Kanel P, van Laar T, Bohnen NI. Cholinergic denervation patterns across cognitive domains in Parkinson's disease. *Mov Disord.* 2021;36:642–650.
26. Sanchez-Catasus CA, Bohnen NI, Yeh FC, D'Cruz N, Kanel P, Müller MLTM. Dopaminergic nigrostriatal connectivity in early Parkinson disease: in vivo neuroimaging study of ^{11}C-DTBZ PET combined with correlational tractography. *J Nucl Med.* 2021;62:545–552.
27. Legault-Denis C, Aghourian M, Soucy JP, et al. Normal cognition in Parkinson's disease may involve hippocampal cholinergic compensation: an exploratory PET imaging study with [^{18}F]-FEOBV. *Parkinsonism Relat Disord.* 2021;91:162–166.
28. Jørgensen NP, Alstrup AK, Mortensen FV, et al. Cholinergic PET imaging in infections and inflammation using ^{11}C-donepezil and ^{18}F-FEOBV. *Eur J Nucl Med Mol Imaging.* 2017;44:449–458.
29. Gotti C, Moretti M, Gaimarri A, Zanardi A, Clementi F, Zoli M. Heterogeneity and complexity of native brain nicotinic receptors. *Biochem Pharmacol.* 2007;74: 1102–1111.
30. Court JA, Martin-Ruiz C, Graham A, Perry E. Nicotinic receptors in human brain: topography and pathology. *J Chem Neuroanat.* 2000;20:281–298.
31. Paterson D, Nordberg A. Neuronal nicotinic receptors in the human brain. *Prog Neurobiol.* 2000;61:75–111.
32. Shimohama S, Taniguchi T, Fujiwara M, Kameyama M. Changes in nicotinic and muscarinic cholinergic receptors in Alzheimer-type dementia. *J Neurochem.* 1986;46:288–293.
33. Laikowski MM, Reisdorfer F, Moura S. NAChR $\alpha4\beta2$ subtype and their relation with nicotine addiction, cognition, depression and hyperactivity disorder. *Curr Med Chem.* 2019;26:3792–3811.
34. Flynn DD, Mash DC. Characterization of L-[^{3}H]nicotine binding in human cerebral cortex: comparison between Alzheimer's disease and the normal. *J Neurochem.* 1986;47:1948–1954.
35. Nordberg A, Winblad B. Reduced number of [^{3}H]nicotine and [^{3}H]acetylcholine binding sites in the frontal cortex of Alzheimer brains. *Neurosci Lett.* 1986;72: 115–119.
36. Perry E, Martin-Ruiz C, Lee M, et al. Nicotinic receptor subtypes in human brain ageing, Alzheimer and Lewy body diseases. *Eur J Pharmacol.* 2000;393: 215–222.
37. Perry EK, Morris CM, Court JA, et al. Alteration in nicotine binding sites in Parkinson's disease, Lewy body dementia and Alzheimer's disease: possible index of early neuropathology. *Neuroscience.* 1995;64:385–395.
38. Pimlott SL, Piggott M, Owens J, et al. Nicotinic acetylcholine receptor distribution in Alzheimer's disease, dementia with Lewy bodies, Parkinson's disease, and vascular dementia: in vitro binding study using 5-[^{125}I]-a-85380. *Neuropsychopharmacology.* 2004;29:108–116.
39. Schmaljohann J, Gündisch D, Minnerop M, et al. In vitro evaluation of nicotinic acetylcholine receptors with 2-[^{18}F]F-A85380 in Parkinson's disease. *Nucl Med Biol.* 2006;33:305–309.
40. Sihver W, Gillberg PG, Svensson AL, Nordberg A. Autoradiographic comparison of [^{3}H](−)nicotine, [^{3}H]cytisine and [^{3}H]epibatidine binding in relation to vesicular acetylcholine transport sites in the temporal cortex in Alzheimer's disease. *Neuroscience.* 1999;94:685–696.
41. Whitehouse PJ, Martino AM, Antuono PG, et al. Nicotinic acetylcholine binding sites in Alzheimer's disease. *Brain Res.* 1986;371:146–151.
42. Lao PJ, Betthauser TJ, Tudorascu DL, et al. [^{18}F]nifene test-retest reproducibility in first-in-human imaging of $\alpha4\beta2$* nicotinic acetylcholine receptors. *Synapse.* 2017;71:10.1002/syn.21981.
43. Wong DF, Kuwabara H, Kim J, et al. PET imaging of high-affinity $\alpha4\beta2$ nicotinic acetylcholine receptors in humans with ^{18}F-AZAN, a radioligand with optimal brain kinetics. *J Nucl Med.* 2013;54:1308–1314.

44. Sabri O, Becker GA, Meyer PM, et al. First-in-human PET quantification study of cerebral $\alpha4\beta2$* nicotinic acetylcholine receptors using the novel specific radioligand (−)-[^{18}F]flubatine. *Neuroimage.* 2015;118:199–208.
45. Sabri O, Meyer PM, Gräf S, et al. Cognitive correlates of $\alpha4\beta2$ nicotinic acetylcholine receptors in mild Alzheimer's dementia. *Brain.* 2018;141:1840–1854.
46. Coughlin JM, Slania S, Du Y, et al. ^{18}F-XTRA PET for enhanced imaging of the extrathalamic $\alpha4\beta2$ nicotinic acetylcholine receptor. *J Nucl Med.* 2018;59:1603–1608.
47. Tiepolt S, Becker G-A, Wilke S, et al. (+)-[^{18}F]flubatine as a novel $\alpha4\beta2$ nicotinic acetylcholine receptor PET ligand: results of the first-in-human brain imaging application in patients with β-amyloid PET-confirmed Alzheimer's disease and healthy controls. *Eur J Nucl Med Mol Imaging.* 2021;48:731–746.
48. Mukhin AG, Kimes AS, Chefer SI, et al. Greater nicotinic acetylcholine receptor density in smokers than in nonsmokers: a PET study with 2-^{18}F-FA-85380. *J Nucl Med.* 2008;49:1628–1635.
49. Brody AL, Mandelkern MA, London ED, et al. Cigarette smoking saturates brain alpha 4 beta 2 nicotinic acetylcholine receptors. *Arch Gen Psychiatry.* 2006;63:907–915.
50. Bhatt S, Hillmer AT, Nabulsi N, et al. Evaluation of (−)-[^{18}F]flubatine-specific binding: implications for reference region approaches. *Synapse.* 2018;72:10.1002/syn.22016.
51. Sabri O, Kendziorra K, Wolf H, Gertz HJ, Brust P. Acetylcholine receptors in dementia and mild cognitive impairment. *Eur J Nucl Med Mol Imaging.* 2008;35(suppl 1)S30–S45.
52. Kendziorra K, Wolf H, Meyer PM, et al. Decreased cerebral $\alpha4\beta2$* nicotinic acetylcholine receptor availability in patients with mild cognitive impairment and Alzheimer's disease assessed with positron emission tomography. *Eur J Nucl Med Mol Imaging.* 2011;38:515–525.
53. Okada H, Ouchi Y, Ogawa M, et al. Alterations in $\alpha4\beta2$ nicotinic receptors in cognitive decline in Alzheimer's aetiopathology. *Brain.* 2013;136:3004–3017.
54. Sultzer DL, Melrose RJ, Riskin-Jones H, et al. Cholinergic receptor binding in Alzheimer disease and healthy aging: assessment in vivo with positron emission tomography imaging. *Am J Geriatr Psychiatry.* 2017;25:342–353.
55. Fujita M, Ichise M, Zoghbi SS, et al. Widespread decrease of nicotinic acetylcholine receptors in Parkinson's disease. *Ann Neurol.* 2006;59:174–177.
56. O'Brien JT, Colloby SJ, Pakrasi S, et al. Nicotinic $\alpha4\beta2$ receptor binding in dementia with Lewy bodies using ^{123}I-5IA-85380 SPECT demonstrates a link between occipital changes and visual hallucinations. *Neuroimage.* 2008;40:1056–1063.
57. Kas A, Bottlaender M, Gallezot JD, et al. Decrease of nicotinic receptors in the nigrostriatal system in Parkinson's disease. *J Cereb Blood Flow Metab.* 2009;29:1601–1608.
58. Meyer PM, Strecker K, Kendziorra K, et al. Reduced $\alpha4\beta2$*-nicotinic acetylcholine receptor binding and its relationship to mild cognitive and depressive symptoms in Parkinson disease. *Arch Gen Psychiatry.* 2009;66:866–877.
59. Lorenz R, Samnick S, Dillmann U, et al. Nicotinic $\alpha4\beta2$ acetylcholine receptors and cognitive function in Parkinson's disease. *Acta Neurol Scand.* 2014;130:164–171.
60. Isaias IU, Spiegel J, Brumberg J, et al. Nicotinic acetylcholine receptor density in cognitively intact subjects at an early stage of Parkinson's disease. *Front Aging Neurosci.* 2014;6:213.
61. Breese CR, Adams C, Logel J, et al. Comparison of the regional expression of nicotinic acetylcholine receptor $\alpha7$ mRNA and [^{125}I]-alpha-bungarotoxin binding in human postmortem brain. *J Comp Neurol.* 1997;387:385–398.
62. Wang H, Yu M, Ochani M, et al. Nicotinic acetylcholine receptor $\alpha7$ subunit is an essential regulator of inflammation. *Nature.* 2003;421:384–388.
63. Dajas-Bailador FA, Mogg AJ, Wonnacott S. Intracellular Ca2+ signals evoked by stimulation of nicotinic acetylcholine receptors in SH-SY5Y cells: contribution of voltage-operated Ca2+ channels and Ca2+ stores. *J Neurochem.* 2002;81:606–614.
64. Wu J, Ishikawa M, Zhang J, Hashimoto K. Brain imaging of nicotinic receptors in Alzheimer's disease. *Int J Alzheimers Dis.* 2010;2010:548913.
65. Ikonomovic MD, Wecker L, Abrahamson EE, et al. Cortical $\alpha7$ nicotinic acetylcholine receptor and β-amyloid levels in early Alzheimer disease. *Arch Neurol.* 2009;66:646–651.
66. Wang HY, Lee DH, D'Andrea MR, Peterson PA, Shank RP, Reitz AB. β-amyloid(1-42) binds to $\alpha7$ nicotinic acetylcholine receptor with high affinity: implications for Alzheimer's disease pathology. *J Biol Chem.* 2000;275:5626–5632.
67. O'Neill MJ, Murray TK, Lakics V, Visanji NP, Duty S. The role of neuronal nicotinic acetylcholine receptors in acute and chronic neurodegeneration. *Curr Drug Targets CNS Neurol Disord.* 2002;1:399–411.
68. Dziewczapolski G, Glogowski CM, Masliah E, Heinemann SF. Deletion of the $\alpha7$ nicotinic acetylcholine receptor gene improves cognitive deficits and synaptic pathology in a mouse model of Alzheimer's disease. *J Neurosci.* 2009;29:8805–8815.
69. Toyohara J, Sakata M, Wu J, et al. Preclinical and the first clinical studies on [^{11}C]CHIBA-1001 for mapping $\alpha7$ nicotinic receptors by positron emission tomography. *Ann Nucl Med.* 2009;23:301–309.
70. Ishikawa M, Sakata M, Toyohara J, et al. Occupancy of $\alpha7$ nicotinic acetylcholine receptors in the brain by tropisetron: a positron emission tomography study using ^{11}C-CHIBA-1001 in healthy human subjects. *Clin Psychopharmacol Neurosci.* 2011;9:111–116.
71. Brust P, Deuther-Conrad W, Donat C, et al. Preclinical and clinical aspects of nicotinic acetylcholine receptor imaging. In: Dierckx RA, Otte A, de Vries EF, van Waarde A, Lammertsma AA, eds. *PET and SPECT of Neurobiological Systems.* Springer International Publishing; 2021:593–660.
72. Brust P, Peters D, Deuther-Conrad W. Development of radioligands for the imaging of $\alpha7$ nicotinic acetylcholine receptors with positron emission tomography. *Curr Drug Targets.* 2012;13:594–601.
73. Coughlin JM, Du Y, Rosenthal HB, et al. The distribution of the $\alpha7$ nicotinic acetylcholine receptor in healthy aging: an in vivo positron emission tomography study with [^{18}F]ASEM. *Neuroimage.* 2018;165:118–124.
74. Ogawa M, Tsukada H, Hatano K, Ouchi Y, Saji H, Magata Y. Central in vivo nicotinic acetylcholine receptor imaging agents for positron emission tomography (PET) and single photon emission computed tomography (SPECT). *Biol Pharm Bull.* 2009;32:337–340 .
75. Ogawa M, Nishiyama S, Tsukada H, et al. Synthesis and evaluation of new imaging agent for central nicotinic acetylcholine receptor $\alpha7$ subtype. *Nucl Med Biol.* 2010;37:347–355.
76. Nakaizumi K, Ouchi Y, Terada T, et al. In vivo depiction of $\alpha7$ nicotinic receptor loss for cognitive decline in Alzheimer's disease. *J Alzheimers Dis.* 2018;61:1355–1365.
77. Coughlin JM, Rubin LH, Du Y, et al. High availability of the $\alpha7$-nicotinic acetylcholine receptor in brains of individuals with mild cognitive impairment: a pilot study using ^{18}F-ASEM PET. *J Nucl Med.* 2020;61:423–426.
78. Thomsen M, Sørensen G, Dencker D. Physiological roles of CNS muscarinic receptors gained from knockout mice. *Neuropharmacology.* 2018;136:411–420.
79. Eckelman WC. Imaging of muscarinic receptors in the central nervous system. *Curr Pharm Des.* 2006;12:3901–3913.
80. Assous M. Striatal cholinergic transmission: focus on nicotinic receptors' influence in striatal circuits. *Eur J Neurosci.* 2021;53:2421–2442.
81. Lebois EP, Thorn C, Edgerton JR, Popiolek M, Xi S. Muscarinic receptor subtype distribution in the central nervous system and relevance to aging and Alzheimer's disease. *Neuropharmacology.* 2018;136:362–373.
82. Flynn DD, Ferrari-DiLeo G, Mash DC, Levey AI. Differential regulation of molecular subtypes of muscarinic receptors in Alzheimer's disease. *J Neurochem.* 1995;64:1888–1891.
83. Tsang SWY, Lai MKP, Kirvell S, et al. Impaired coupling of muscarinic M1 receptors to G-proteins in the neocortex is associated with severity of dementia in Alzheimer's disease. *Neurobiol Aging.* 2006;27:1216–1223.
84. Yi JH, Whitcomb DJ, Park SJ, et al. M1 muscarinic acetylcholine receptor dysfunction in moderate Alzheimer's disease pathology. *Brain Commun.* 2020;2:fcaa058.
85. Brugnoli A, Pisanò CA, Morari M. Striatal and nigral muscarinic type 1 and type 4 receptors modulate levodopa-induced dyskinesia and striato-nigral pathway activation in 6-hydroxydopamine hemilesioned rats. *Neurobiol Dis.* 2020;144:105044.
86. Ztaou S, Maurice N, Camon J, et al. Involvement of striatal cholinergic interneurons and M1 and M4 muscarinic receptors in motor symptoms of Parkinson's disease. *J Neurosci.* 2016;36:9161–9172.
87. Araujo DM, Lapchak PA, Robitaille Y, Gauthier S, Quirion R. Differential alteration of various cholinergic markers in cortical and subcortical regions of human brain in Alzheimer's disease. *J Neurochem.* 1988;50:1914–1923.
88. Mash DC, Flynn DD, Potter LT. Loss of M2 muscarine receptors in the cerebral cortex in Alzheimer's disease and experimental cholinergic denervation. *Science.* 1985;228:1115–1117.
89. Moran SP, Maksymetz J, Conn PJ. Targeting muscarinic acetylcholine receptors for the treatment of psychiatric and neurological disorders. *Trends Pharmacol Sci.* 2019;40:1006–1020.
90. McOmish C, Pavey G, McLean C, Horne M, Dean B, Scarr E. Muscarinic receptor binding changes in postmortem Parkinson's disease. *J Neural Transm.* 2017;124:227–236.
91. Ozenil M, Aronow J, Millard M, et al. Update on PET tracer development for muscarinic acetylcholine receptors. *Pharmaceuticals (Basel).* 2021;14:530.
92. Naganawa M, Nabulsi N, Henry S, et al. First-in-human assessment of ^{11}C-LSN3172176, an M1 muscarinic acetylcholine receptor PET radiotracer. *J Nucl Med.* 2021;62:553–560.
93. Cannon DM, Carson RE, Nugent AC, et al. Reduced muscarinic type 2 receptor binding in subjects with bipolar disorder. *Arch Gen Psychiatry.* 2006;63:741–747.

94. Ravasi L, Tokugawa J, Nakayama T, et al. Imaging of the muscarinic acetylcholine neuroreceptor in rats with the M2 selective agonist [^{18}F]FP-TZTP. *Nucl Med Biol.* 2012;39:45–55.
95. Ichise M, Cohen RM, Carson RE. Noninvasive estimation of normalized distribution volume: application to the muscarinic-2 ligand [^{18}F]FP-TZTP. *J Cereb Blood Flow Metab.* 2008;28:420–430.
96. Tong L, Li W, Lo MM, et al. Discovery of [^{11}C]MK-6884: a positron emission tomography (PET) imaging agent for the study of M4 muscarinic receptor positive allosteric modulators (PAMs) in neurodegenerative diseases. *J Med Chem.* 2020;63:2411–2425.
97. Li W, Wang Y, Lohith TG, et al. The PET tracer [^{11}C]MK-6884 quantifies M4 muscarinic receptor in rhesus monkeys and patients with Alzheimer's disease. *Sci Transl Med.* 2022;14:eabg3684.
98. Rowe CC, Krishnadas N, Ackermann U, et al. PET imaging of brain muscarinic receptors with ^{18}F-fluorobenzyl-dexetimide: a first in human study. *Psychiatry Res Neuroimaging.* 2021;316:111354.
99. Colloby SJ, Nathan PJ, McKeith IG, Bakker G, O'Brien JT, Taylor JP. Cholinergic muscarinic M_1/M_4 receptor networks in dementia with Lewy bodies. *Brain Commun.* 2020;2:fcaa098.
100. Colloby SJ, McKeith IG, Wyper DJ, O'Brien JT, Taylor JP. Regional covariance of muscarinic acetylcholine receptors in Alzheimer's disease using (R, R) [^{123}I]-QNB SPECT. *J Neurol.* 2015;262:2144–2153.
101. Atack JR, Perry EK, Bonham JR, Candy JM, Perry RH. Molecular forms of acetylcholinesterase and butyrylcholinesterase in the aged human central nervous system. *J Neurochem.* 1986;47:263–277.
102. Bohnen NI, Frey KA. Imaging of cholinergic and monoaminergic neurochemical changes in neurodegenerative disorders. *Mol Imaging Biol.* 2007;9:243–257.
103. Shinotoh H, Hirano S, Shimada H. PET imaging of acetylcholinesterase. In: Dierckx RA, Otte A, de Vries EF, van Waarde A, Lammertsma AA, eds. *PET and SPECT of Neurobiological Systems.* Springer International Publishing; 2020:193–220.
104. Mesulam MM, Geula C. Overlap between acetylcholinesterase-rich and choline acetyltransferase-positive (cholinergic) axons in human cerebral cortex. *Brain Res.* 1992;577:112–120.
105. Irie T, Fukushi K, Akimoto Y, Tamagami H, Nozaki T. Design and evaluation of radioactive acetylcholine analogs for mapping brain acetylcholinesterase (AchE) in vivo. *Nucl Med Biol.* 1994;21:801–808.
106. Irie T, Fukushi K, Namba H, et al. Brain acetylcholinesterase activity: validation of a PET tracer in a rat model of Alzheimer's disease. *J Nucl Med.* 1996;37:649–655.
107. Namba H, Iyo M, Shinotoh H, Nagatsuka S, Fukushi K, Irie T. Preserved acetylcholinesterase activity in aged cerebral cortex. *Lancet.* 1998;351:881–882.
108. Kuhl DE, Koeppe RA, Minoshima S, et al. In vivo mapping of cerebral acetylcholinesterase activity in aging and Alzheimer's disease. *Neurology.* 1999;52:691–699.
109. Bohnen NI, Kanel P, Müller MLTM. Molecular imaging of the cholinergic system in Parkinson's disease. *Int Rev Neurobiol.* 2018;141:211–250.
110. Pasquini J, Brooks DJ, Pavese N. The cholinergic brain in Parkinson's disease. *Mov Disord Clin Pract (Hoboken).* 2021;8:1012–1026.
111. Iyo M, Namba H, Fukushi K, et al. Measurement of acetylcholinesterase by positron emission tomography in the brains of healthy controls and patients with Alzheimer's disease. *Lancet.* 1997;349:1805–1809.
112. Shinotoh H, Namba H, Fukushi K, et al. Progressive loss of cortical acetylcholinesterase activity in association with cognitive decline in Alzheimer's disease: a positron emission tomography study. *Ann Neurol.* 2000;48:194–200.
113. Rinne JO, Kaasinen V, Järvenpää T, et al. Brain acetylcholinesterase activity in mild cognitive impairment and early Alzheimer's disease. *J Neurol Neurosurg Psychiatry.* 2003;74:113–115.
114. Bohnen NI, Kaufer DI, Hendrickson R, et al. Cognitive correlates of alterations in acetylcholinesterase in Alzheimer's disease. *Neurosci Lett.* 2005;380:127–132.
115. Kuhl DE, Minoshima S, Frey KA, Foster NL, Kilbourn MR, Koeppe RA. Limited donepezil inhibition of acetylcholinesterase measured with positron emission tomography in living Alzheimer cerebral cortex. *Ann Neurol.* 2000;48:391–395.
116. Richter N, Beckers N, Onur OA, et al. Effect of cholinergic treatment depends on cholinergic integrity in early Alzheimer's disease. *Brain.* 2018;141:903–915.
117. Gilman S, Koeppe RA, Nan B, et al. Cerebral cortical and subcortical cholinergic deficits in parkinsonian syndromes. *Neurology.* 2010;74:1416–1423.
118. Bohnen NI, Kaufer DI, Ivanco LS, et al. Cortical cholinergic function is more severely affected in parkinsonian dementia than in Alzheimer disease: an in vivo positron emission tomographic study. *Arch Neurol.* 2003;60:1745–1748.
119. Bohnen NI, Kaufer DI, Hendrickson R, et al. Cognitive correlates of cortical cholinergic denervation in Parkinson's disease and parkinsonian dementia. *J Neurol.* 2006;253:242–247.
120. Liu SY, Wile DJ, Fu JF, et al. The effect of LRRK2 mutations on the cholinergic system in manifest and premanifest stages of Parkinson's disease: a cross-sectional PET study. *Lancet Neurol.* 2018;17:309–316.